SCIENTIFIC CULTURE
www.sci-cult.com

SCIENTIFIC CULTURE, Vol. 12, No. 2.1, (2026), pp. 5248-5267
Open Access. Online & Print

DOI: 10.5281/zenodo.19114308

PREHISTORIC SEA-LEVEL CHANGE AND MEDIEVAL RECORDS OF EXTREME WAVES FROM THE ANDAMAN COAST OF THE THAI-MALAY PENINSULA IN GEOMORPHOLOGICAL AND ARCHAEOLOGICAL CONTEXTS

Stapana Kongsen[1], Chanakan Ketthong[1*], Sirawat Udomsak[1], Chanista Chansom[2], Peerasit Surakiatchai[3], Patcharaporn Ngernkerd[4], Nutcha Choowong[5], Norakrit Butkaew[2], Peerasak Klubket[2], Kantapon Suraprasit[1], Sumet Phantuwongraj[1], Santi Pailoplee[1], Akkaneewut Jirapinyakul[1], Vichai Chutakositkanon[1] and Montri Choowong[1*]

[1] Center of Excellence for the Morphology of Earth Surface and Advanced Geohazards in Southeast Asia (MESA CE), Department of Geology, Faculty of Science, Chulalongkorn University, Bangkok, Thailand
[2] Department of Geology, Faculty of Science, Chulalongkorn University, Bangkok, Thailand
[3] College of Public Health Sciences, Chulalongkorn University, Bangkok, Thailand
[4] Department of Archaeology, Faculty of Archaeology, Silpakorn University, Bangkok, Thailand
[5] Department of Geography, Faculty of Arts, Chulalongkorn University, Bangkok, Thailand

Received: 06/02/2026
Accepted: 05/03/2026

Corresponding Authors: Montri Choowong, Chanakan Ketthong (Montri.c@chula.ac.th; one.chanakan@gmail.com)

ABSTRACT

Beach ridge plains, small islands, estuaries and bay along the Andaman coast of the Thai–Malay Peninsula (TMP) constitute dynamic environmental change where extreme coastal hazards and maritime waypoints have long intersected since the prehistoric to medieval period. While commonly interpreted as geomorphological responses to mid–late Holocene sea-level fluctuations, these coastal landforms also preserve material traces of how past societies lived with an unstable and hazard-prone sea. This study investigates prehistoric to medieval sea-level changes and extreme wave events recorded within the beach ridge–swale complex of Lanta Island (LI) and Phrathong Island (PTI), southwestern Thailand, integrating geomorphological evidence with archaeological indicators nearby. Sedimentological and stratigraphical characteristics of beach ridges and washover deposits were analyzed, and a chronological framework was established using optically stimulated luminescence (OSL) dating. These records were compared with evidence from PTI to identify regional patterns of coastal evolution and the recurrence of extreme coastal hazards, including tsunamis and severe storms. Three stratigraphic layers indicative of extreme wave events were identified within the outer swales of the beach ridge plain on PTI whereas one modern storm overwash and the 2004 tsunami deposit found at LI. In parallel, prehistoric rock paintings were documented on cliff walls of Limestone Island within the Lanta Bay, with their elevations ranging from 3.6 to 7.7 m above present sea level measured using high precision field method and terrestrial LiDAR survey. Together, these geomorphological and archaeological records reveal a long history of living with the sea, in which shifting shorelines, extreme waves, and maritime connectivity shaped coastal landscapes, memory, and human–environment relationships from prehistory to the present.

KEYWORDS: Holocene Sea Level Change, Extreme Coastal Hazards, Rock Art Archaeology, Maritime Waypoints, Lanta Island, Sailboat Painting.

1. INTRODUCTION

Studies that integrate archaeological evidence with sedimentological records and historical documentation remain relatively limited, despite their potential to provide a more comprehensive understanding of past coastal hazards. A notable example is Atwater et al. (2005), The Orphan Tsunami of 1700, which successfully reconstructed a historical tsunami through the synthesis of geological and documentary evidence. Coastal zones along the Andaman coast of the Thai–Malay Peninsula (TMP) have long functioned as dynamic interfaces where environmental change, extreme coastal hazards, and human maritime lifeways intersect. Rather than static boundaries, these coasts represent evolving cultural landscapes shaped by shifting sea levels, episodic high-energy waves, and sustained maritime interaction. Several beach ridge plains from the Andaman coast were determined the age of beach to have formed in the prehistoric to the present period. Some of them were younger than some archaeological sites. Therefore, understanding how past societies lived with an unstable and hazard-prone sea requires an integrated perspective that considers geomorphological processes alongside archaeological evidence and culturally meaningful seascapes.

In this study, we focused on how the formation of beach ridge plains during the prehistoric to medieval period intersect among the archaeological evidence. We approached the interconnection among geology, geography and archaeology based solely on scientific analysis including sedimentological, chronological and geochemistry perspectives. Beach ridge plains are back-barrier coastal systems that form through shoreline progradation and are characterized by elongate, wave-built sand ridges separated by low-lying swales. These systems are widely recognized for their capacity to preserve washover sediments associated with extreme wave events, such as tsunamis and severe storms. The progradation rates and internal architecture of beach ridge plains are influenced by fluvial sediment supply, aeolian transport driven by onshore winds, and longer-term climatic variability (Tamura, 2012). As relative sea level gradually changes, successive beach ridges accrete seaward; while intervening swales act as sediment traps that preserve deposits from both recent and prehistoric extreme wave events, providing valuable chronological archives of paleoenvironments and coastal instability.

In Southeast Asia, beach ridge–swale complexes are widely distributed along Holocene coastlines of the TMP (Choowong, 2011; Nimnate et al., 2015; Brill et al., 2015; Polwichai et al., 2023; Laerosa et al., 2024). The western margin of the peninsula faces the Andaman Sea and lies close to the India–Australia subduction zone, where megathrust earthquakes have generated large tsunamis, most notably the 26 December 2004 Sumatra–Andaman event (Mw 9.1–9.3) that devastated much of the Andaman coast (Lay et al., 2005; Satake et al., 2006; Stein and Okal, 2007; Chlieh et al., 2007). In contrast, the eastern side of the peninsula, bordering the Gulf of Thailand (GoT), is affected by tropical cyclones, highlighting the dual exposure of the TMP to different extreme coastal hazards. These geological and climatic settings make the region particularly suitable for investigating the sedimentology and chronology of washover deposits preserved within beach ridge plains.

Following the 2004 Indian Ocean Tsunami (2004 IOT), extensive tsunami sands were deposited along the Andaman coast, especially within swales between beach ridges (Hawkes et al., 2007; Choowong et al., 2007; Fujino et al., 2009; Sawai et al., 2009; Naruse et al., 2010). Subsequent studies have documented the sedimentological characteristics of these deposits at numerous sites along the northern Thai littoral zone, including Phra Thong Island (PTI), Kho Khao Island (KKI), Pakarang Cape, Tap Lamu Beach, and Kamala Beach (Choowong et al., 2007; Choowong et al., 2008a, b; Jankaew et al., 2008; Feldens et al., 2009; Goto et al., 2012; Fujino et al., 2016, 2018). These studies have significantly advanced understanding of tsunami sedimentation and recurrence; however, detailed sedimentological and chronological investigations remain limited for several beach ridge plains in the southern Andaman coast, particularly around Phuket and adjacent islands.

Lanta Island (LI) represents a promising yet understudied beach ridge–swale complex for examining long-term coastal evolution and extreme wave records. Its geomorphology and local topography exert strong controls on sediment preservation within swales, offering an opportunity to integrate high-resolution coastal geomorphology with archaeological evidence, rock art, and maritime networks. By situating beach ridge plains within a broader cultural and historical seascape, this study seeks to bridge physical and humanities-oriented approaches and to explore how sea-level change, extreme coastal hazards, and maritime interaction co-evolved along the Andaman coast from prehistory to the medieval period.

2. GEOGRAPHICAL AND GEOLOGICAL SETTINGS

Geographically, LI and PTI are located along the Andaman coast on the western TMP (Figs. 1a, b). PTI lies in Phang-Nga Province, approximately 130 km north of Phuket, while LI is in Krabi Province, about 70 km southeast of Phuket. Both islands exhibit similar geomorphological settings, with beach ridge plains along the west coast and mangrove forests facing embayments on the east, reflecting the interaction between marine processes and terrestrial sediment supply. The west coast of the TMP is characterized by a steep shoreline with rocky headlands and mainland cliffs. At LI and PTI, the Quaternary coastal plains consist of intertidal flats and sandy beach-ridge plains, where large tidal channels directly deliver mainland sediments to the shore. The offshore bathymetry of the Andaman Sea shelf is underlain by weathered granitic rocks, and the seafloor sediments show a gentle seaward gradient. PTI and LI exhibit similar landform characteristics. The inner or eastern parts of both islands are developed as small barrier-island systems, separated from the mainland by tidal channels. PTI extends approximately 15 km from north to south and up to 8 km in an east–west direction. Although the TMP is located close to the seismically active Sumatra–Andaman subduction zone, it is regarded as tectonically relatively stable (Tjia, 1996).

LI consists of two main parts: Lanta Noi in the north and Lanta Yai in the south, separated by a tidal channel (Fig. 2a). Lanta Yai forms a cuspate headland composed of Carboniferous–Permian clastic sedimentary rocks extending into the Andaman Sea, whereas Lanta Noi is largely covered by Quaternary marine clay and mangrove forests. The northwest quadrant of LI hosts beach ridge plains covering approximately 4.5 km², which remain undated. The eastern region of LI faces an embayment near the mainland, underlain by similar Carboniferous–Permian rocks, influencing local sediment deposition and hydrodynamics.

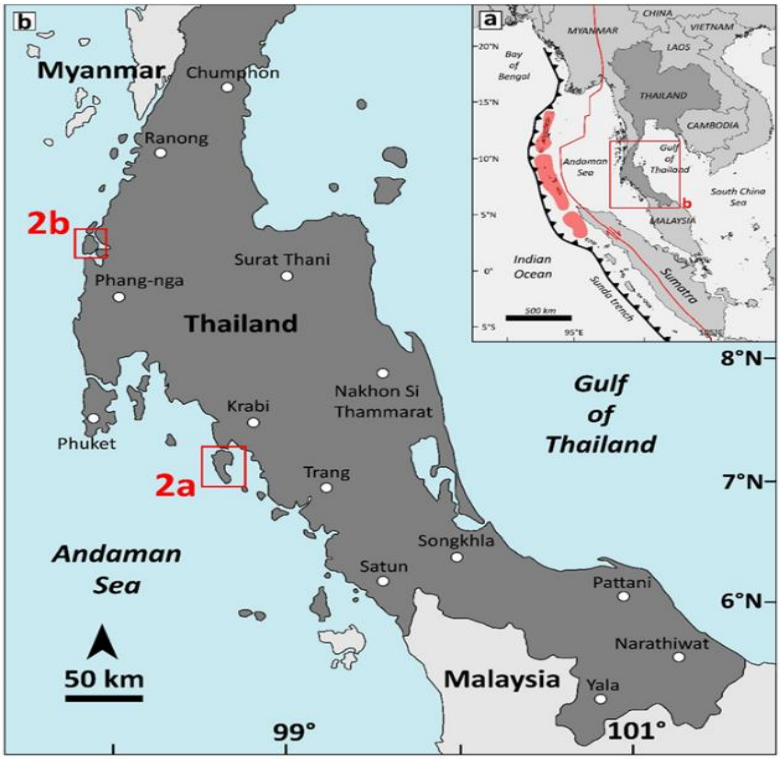

Figure 1: Study sites. (a) Southeast Asia region showing the Sunda Trench (thick black line with triangles) and the Sumatra Fault (red line). (b) The Thai-Malay Peninsula (TMP) and study areas corresponding to panels 2a and 2b.

PTI is primarily covered by Quaternary beach sediments, including sand ridges and runnels, with small islands and rock exposures in the northwest (Fig. 2b). Ridges, rising 3–5 m above mean sea level (MSL), have formed over the last 6,000 years (Lansai, 2004; Gouramanis et al., 2014, 2015, 2017; Brill et al., 2015). Interspersed swales have preserved the 2004 IOT sand sheet and multiple paleo-tsunami layers (Jankaew et al., 2008; Fujino et al., 2008). Both islands are situated between 7°15′N and 9°15′N, less than 10° from the equator, where the Coriolis effect limits cyclonic wind intensity (Jankaew et al., 2008). They

experience annual southwest monsoons, with PTI more exposed to open-sea conditions. During the 2004 IOT, maximum wave heights at LI reached 5–6 m, with run-ups up to 10 m, causing extensive overwash, vegetation loss, and infrastructure damage within Mu Ko Lanta Marine National Park (Choowong et al., 2007). PTI, by contrast, experienced inundation up to 2 km inland with waves reaching 10 m (Choowong et al., 2007; Jankaew et al., 2008; Fujino et al., 2008; Brill et al., 2012).

3. METHODOLOGY

3.1 Field data collection

Fieldwork was conducted on LI and PTI to investigate the sedimentology and chronology of beach ridge–swale complexes. On LI, an east–west shore-normal transect was established, extending from the active swash zone to the landward limit (Fig. 2c). Fifteen shallow test pits were excavated to collect sand samples for OSL dating, with samples taken 20–30 cm below the surface and excavation depths limited to 40–50 cm due to the high-water table. A single deep core, 152 cm, was obtained at LT1 and selected for detailed sedimentological analysis. On PTI, gouge cores were used to collect sediments from the beach ridge plain, particularly within swales and low-lying swamp areas. Five cores, 70–90 cm in depth, were described in detail and logged immediately after extraction (Fig. 2d). High-resolution photographs and descriptive logs were produced for all cores and test pits.

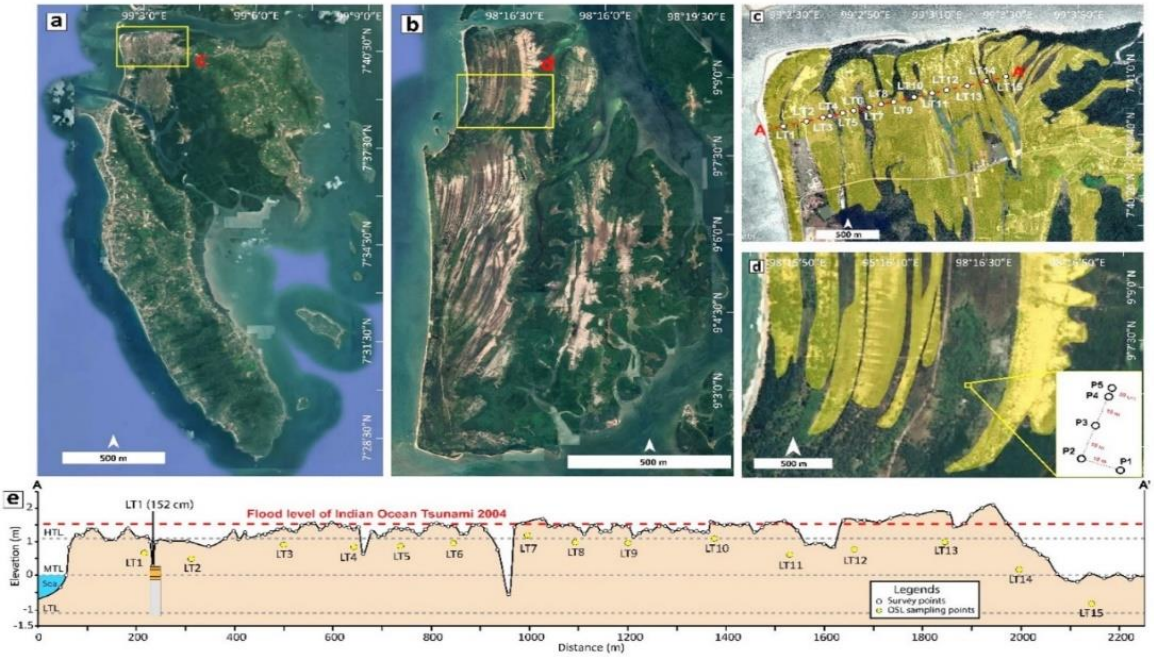

Figure 2: Close-up of study sites with sample locations. (a) Lanta Island (LI). (b) Phra Thong Island (PTI). (c, d) Close-ups of the beach ridge plains on LI and PTI, respectively. (e) High-precision topography along the LI transect with locations of OSL datings and long coring (LT1).

Topographic data on LI beach ridge plain transect were collected using a SOKKIA SET630R total station in fine-average mode, paired with a single-prism reflector. Each survey station was geo-referenced with a handheld Global Positioning System (GPS) receiver, and elevations were normalized to a common vertical datum using the contemporaneous tide record from the Pak Nam Krabi tide-gauge station (Fig. 2e). These data were integrated with sedimentological and chronological analyses to reconstruct beach ridge evolution and infer past extreme wave events. In parallel, prehistoric rock paintings were documented on limestone cliff walls within the marine zone, with their elevations 3.6-7.7 m above present sea level measured using terrestrial LiDAR survey, providing high-resolution vertical profiles. Rock Art Enhancer version 3.8 offered by BinaryEarth were applied for several techniques including decorrelation stretching, histogram equalization, saturation enhancement, and hue/brightness matching to enhance the colours in rock art.

3.2 Grain size, loss on ignition (LOI) analyses

Grain size analysis was conducted at the Sedimentological Laboratory, Geologisches Institute, University of Freiburg, Germany. Sediment samples were analyzed using a Mastersizer 3000 (Malvern

Instruments Limited, Malvern, UK). Each 1 cm interval of sand samples was dispersed in water. Laser obscuration was maintained between 5% and 15%. Prior to measurement, samples were subjected to 10 seconds of ultrasonication to disperse finer grains surrounding the sand particles. Each sample was analyzed three times, and the results were averaged.

Loss on ignition (LOI) analysis was conducted to quantify organic and carbonate contents. Samples were first dried and ground by hand to ensure homogeneity. Approximately 1 g of each sample was weighed and placed in crucibles. A high-temperature furnace (Nabertherm® muffle furnace LE 6/11) was used following the LOI protocol (Heiri et al., 2001). Organic content was determined by heating the samples at 550°C for 4 hours, followed by reweighing. Subsequently, the same samples were heated at 950°C for 1 hour to determine carbonate content. Results were presented along the vertical depth profile from top to bottom.

3.3 Optically stimulated luminescence (OSL) dating

OSL sampling point were aligned on the beach ridges perpendicular to the present shoreline (See location of sample point in Fig. 2c). All the OSL samples was collected using the protected-light plastic tubes for equivalent dose sample (De). A portion of De samples was weighed to determine water content before drying at 105°C. Another portion was oven-dried and sieved through an 841 µm sieve (mesh 120) and a pan. Approximately 290 g of the sieved sample in the pan was weighed and packed into a suitable container for at least one month. Subsequently, natural radioisotope concentrations were measured using high-resolution gamma spectrometry (Canberra). The obtained data, including uranium (ppm), thorium (ppm), and potassium (%), were analyzed based on a standard table (Bell, 1979), and the cosmic ray dose rate was calculated.

For the De chemical preparation, samples were handled in a subdued red-light room at the Sedimentological Laboratory, Chulalongkorn University, to avoid light exposure. Sediments were wet-sieved and cleaned using 125 µm (mesh 120) and 180 µm (mesh 80) sieves to obtain the sand fraction in the 125–180 µm range (Preusser et al., 2008). The sieved samples were submerged in 10% (v/v) HCl to remove carbonate content until the reaction ceased and then rinsed three times with deionized water. Samples were then treated with 30% (v/v) H_2O_2 overnight to eliminate organic matter and rinsed three times with clean water. Subsequently, samples were etched with 40% (v/v) HF for 60 minutes to dissolve feldspar minerals, followed by thorough cleaning and three rinses with deionized water. De samples were dried in an oven at 40°C for 48 hours and stored in light-proof containers. An iso-dynamic magnetic separator was then used to remove ferro-minerals from the dried aliquots. The resulting aliquots were placed on 10 mm diameter stainless steel discs coated with silicone oil. Luminescence signals were measured using a Risø TL/OSL-DA-15C/D reader equipped with an internal $^{90}Sr/^{90}Y$ beta source (ca. 0.102 $Gy \bullet s^{-1}$) and a bialkali EMI photomultiplier. Measurements included a blue diode-pumped laser emitting at 470 nm and a 7.5-mm-thick Hoya U-340 filter. A preheat plateau test was performed prior to measurement. All aliquots were then analyzed using the single-aliquot regenerative (SAR) protocol.

De values were obtained for each sample, with twenty De values measured per sample. All De values were evaluated using Analyst V4.31.7 software. Individual De values were accepted if they met the following criteria: recuperation <5%, recycling ratio within 10%, test dose error <10%, depletion ratio within 10% of unity, adequate fit of the growth curve, and De values enclosed by regenerative doses. Samples failing these criteria were rejected. Dose rate and age calculations were subsequently performed using ADELE v2017 software.

4. RESULTS

4.1 Sedimentology and OSL age of beach ridge plain at LI

The dataset comprises 152 contiguous 1 cm averages of laser-derived mean grain size from the LT1 core (Figs. 2c and 4). Grain sizes range from 2.71 φ (fine sand) to 3.07 φ (very fine sand) (Fig. 3). Sorting in the principal lithofacies spans 0.39 φ (well sorted) to 0.70 φ (moderately well sorted), with two pedogenically disturbed samples (0–1 cm, 1–2 cm) reaching 0.73–0.82 φ (moderately sorted). Skewness exhibits a wide range from –2.89 φ (very coarse skewed) to 0.37 φ (very fine skewed), with the strongest coarse-skewed samples observed near the surface, including –2.89 φ at 0.5 cm and –0.93 φ at 1.5 cm. Kurtosis values mostly fall between 2.3 φ and 2.9 φ (very leptokurtic), with a maximum of 15.43 φ (extremely leptokurtic) at the surface. Most samples contain less than 5% organic matter, whereas the three uppermost samples contain 7–21% organics. Carbonate content is near zero in the upper 55 cm, increasing sharply below this depth, with maximum

values of 6–12% at 85–100 cm.

Based on these sedimentological parameters, five units were identified: Unit A, Unit B, Unit C (upper and lower), Unit D, and Unit E. The characteristics of each unit are summarized in Table 1. Unit A (Topsoil) represents a humic horizon of fine sand located within the upper 9.5 cm below the surface. Most sedimentological parameters are significantly higher than those of the underlying units (Fig. 4b). Mean grain size ranges from 2.77 φ to 3.00 φ, with no systematic upward- or downward-coarsening trend observed. Sorting varies widely, from 0.82 φ at 0.5 cm to ~0.53 φ at 9.5 cm. The uppermost 2 cm are moderately sorted, while the underlying 7 cm grade into moderately well to well-sorted.

Skewness values within this unit are generally fine to very fine skewed. However, near-surface values sharply increase to –2.89 φ at 0.5 cm and –0.93 φ at 1.5 cm, indicating very coarse skewed sediments at the ground surface. Similarly, kurtosis values are markedly higher at the surface, reaching 15.4 φ at 0.5 cm and 5.0 φ at 1.5 cm (extremely leptokurtic), whereas values below mostly fall within the very leptokurtic range of 2.51 φ–2.76 φ.

Unit B is a light-coloured, fine sand layer (2.90 φ–3.00 φ) representing deposits from the 2004 IOT, with a sharp erosional basal contact on the darker underlying substrate (Fig. 4c). This unit is approximately 20 cm thick, ranging from 10 to 32 cm depth. Slight upward fining is observed at the top, with coarsening toward the base. Unit B is well sorted (0.44 φ–0.53 φ), fine to very fine skewed (0.17 φ–0.37 φ), and very leptokurtic (2.32 φ–2.70 φ). Organic matter and carbonate contents are low, both below 5% and 0.1–0.2%, respectively.

Unit C, ranging from 32 to 85 cm, can be subdivided into upper and lower parts, primarily distinguished by carbonate content at ~55 cm depth (Fig. 5a). The upper Unit C is light-coloured and separated from Unit B by a thin, organic-rich layer. Its characteristics are similar to Unit B, including fine to very fine sand (2.79 φ–3.06 φ), well sorted (0.39 φ–0.51 φ), fine to very fine skewed (0.17 φ–0.34 φ), and very leptokurtic (2.34 φ–2.90 φ). Organic matter content increases upward from 0.20% to 5.22%, consistent with a progressive darkening in color. Carbonate content remains near zero. The lower Unit C consists of fine to very fine sand (2.86 φ–2.97 φ), moderately well to well sorted (0.44 φ–0.53 φ), fine skewed (0.16 φ–0.27 φ), and very leptokurtic (2.42 φ–2.71 φ). Organic matter ranges from 0.40% to 1.28%, while carbonate content fluctuates between 0.60% and 6.62%, averaging 2.76%.

Unit D is distinctly highlighted across all parameters within an 8 cm thickness (85–93 cm). Grain size ranges from 2.71 φ to 2.89 φ (fine sand) and exhibits an upward fining trend. Sorting, skewness, and kurtosis fluctuate within moderately well sorted (0.50 φ–0.70 φ), fine to very coarse skewed (–1.25 φ–0.18 φ), and very leptokurtic to extremely leptokurtic (2.66 φ–7.12 φ) ranges. Organic matter content varies from 0.49% to 1.38%. Carbonate content averages 7.81%, peaking at 12.18%, the highest value observed throughout the LT1 core.

Unit E is the lowermost unit, with a maximum thickness of 59 cm, extending from 93 to 152 cm depth. Its sedimentological characteristics closely resemble those of lower Unit C across all parameters. Although the entire unit consists of fine sand, grain size gradually decreases from coarser sand (2.84 φ–2.96 φ at 93.5–119.5 cm) to finer sand (2.97 φ–3.02 φ at 120.5–151.5 cm). Unit E is well sorted (0.40 φ–0.50 φ), fine to very fine skewed (0.16 φ–0.33 φ), and very leptokurtic (2.41 φ–2.90 φ). Organic matter and carbonate contents range from 0.29% to 1.39% and 0.80% to 7.10%, respectively.

OSL dating of beach ridges. The average height of beach ridges at LI is 1.5 m above mean sea level (MSL), with the highest ridge located innermost, exceeding 2 m above MSL. Table 2 summarizes the results of fifteen OSL age determinations (LT1–LT15) collected along the shore-normal beach ridge transect. K, Th, and U concentrations are uniformly low, ranging from 0.05–0.07 wt% K, 0.19–4.78 ppm Th, and 0.18–4.27 ppm U. These values are typical of quartz-rich littoral sands derived from granitic and metasedimentary hinterlands and, after accounting for in-situ water contents (4–14%), correspond to environmental De of 0.29–1.41 Gy ka^{-1}.

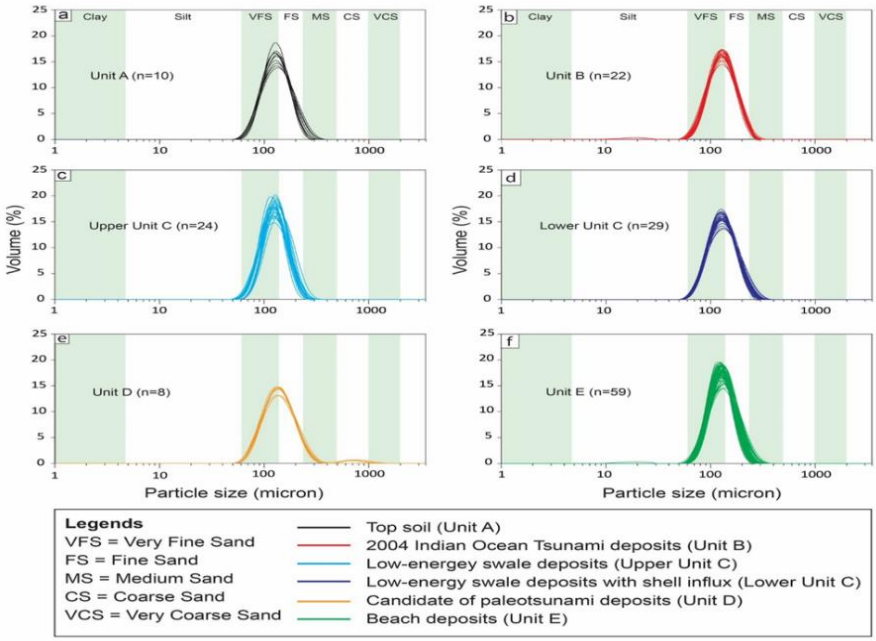

Figure 3: Grain size distribution curves from shore-normal beach ridge, extreme wave sediments found on beach ridge plain. (a) to (f) Particle size (micron) of each sedimentary unit from different layers collected along LI and PTI pits.

One outlier, sample LT1, exhibits elevated radionuclide concentrations and dose rate (1.41 ± 0.02 Gy ka^{-1}) due to the pit intersecting a shell-hash layer rich in Th-bearing heavy minerals. For the remainder of the sequence, the average dose rate is 0.37 ± 0.05 Gy ka^{-1}, providing a relatively uniform dosimetric environment for the interpretation of equivalent doses (D_e).

Aliquot statistics indicate consistently robust luminescence behaviour. Between 16 and 20 aliquots were accepted per sample, with recuperation <5%, recycling ratios within ±10% of unity, and test-dose errors below 10%. Overdispersion (OD) values are uniformly low (0.02–0.25), suggesting minimal residual bleaching at deposition and negligible beta-dose heterogeneity. Consequently, all samples met the criteria for application of the Central Age Model (CAM), and the Minimum Age Model (MAM) was not required.

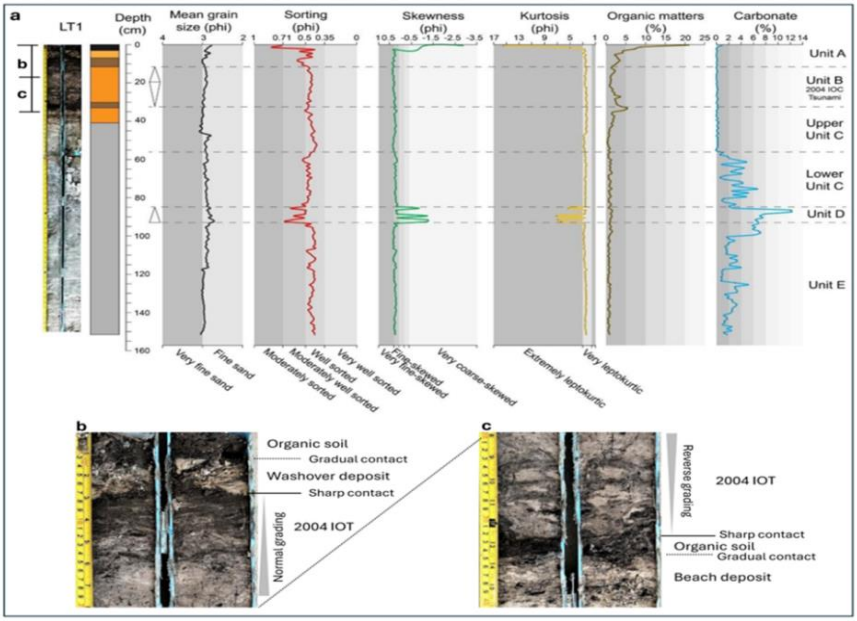

Figure 4: Stratigraphic column with detail of grain size parameters and LOI. Photograph of coring LT1 with visual stratigraphic logging (left). Gray columns indicate detailed analyses of laser granulometry: grain size, sorting, skewness, kurtosis, organic matter, and carbonate content.

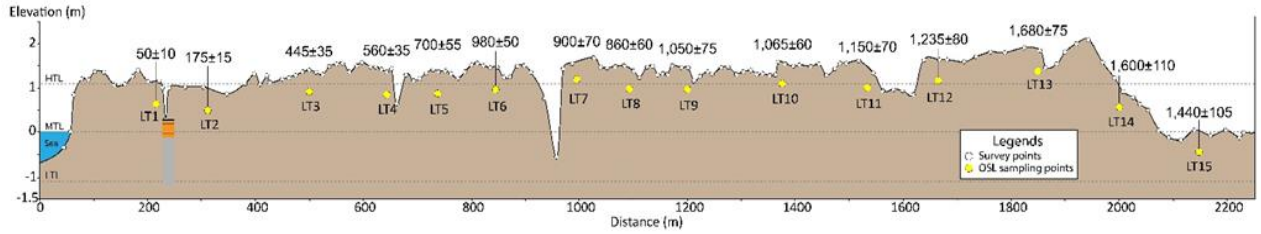

Figure 5: Topographic profile along the LI transects with OSL dating results. Age ranging from 1,680 to 50 years, showing rapid seaward progradation of approximately 1,800 m from east to west.

The youngest sample (LT1) exhibits the highest overdispersion (0.25), as expected for very recent beachface deposits that may contain grains with heterogeneous exposure histories. Nevertheless, the CAM-derived equivalent dose (D_e) of 0.07 ± 0.01 Gy is well constrained. The resulting beach ridge ages range from 1,680 ± 75 to 50 ± 10 years, indicating a depositional chronology during the late Holocene.

The ridges are ordered by age, with the oldest located at the innermost ridge and the youngest at the most recent seaward ridges (Table 1) (Fig. 5).

Table 1: OSL dating results from beach ridge plain of LI.

Sample	K (%)	Th (ppm)	U (ppm)	Water (%)	D (Gy/ka^{-1})	n	od (%)	Model	D_e OSL (Gy)	Age (yr)
LT1	0.06 ± 0.01	4.78 ± 0.06	4.27 ± 0.02	13.44	1.41 ± 0.02	20/18	0.25	CAM	0.07 ± 0.01	50 ± 10
LT2	0.07 ± 0.01	1.69 ± 0.04	1.42 ± 0.01	6.11	0.68 ± 0.06	20817	0.10	CAM	0.12 ± 0.01	175 ± 15
LT3	0.06 ± 0.01	0.64 ± 0.02	0.42 ± 0.01	5.97	0.38 ± 0.03	20/16	0.17	CAM	0.17 ± 0.01	445 ± 35
LT4	0.06 ± 0.01	0.72 ± 0.03	0.67 ± 0.01	5.2	0.45 ± 0.04	20/17	0.17	CAM	0.25 ± 0.01	560 ± 35
LT5	0.05 ± 0.01	0.69 ± 0.02	0.24 ± 0.01	10.36	0.33 ± 0.03	20/19	0.17	CAM	0.23 ± 0.01	700 ± 55
LT6	0.06 ± 0.01	0.99 ± 0.03	0.59 ± 0.01	4.3	0.45 ± 0.03	20/20	0.13	CAM	0.44 ± 0.01	980 ± 50
LT7	0.05 ± 0.01	0.19 ± 0.01	0.18 ± 0.01	5.47	0.29 ± 0.02	20/20	0.08	CAM	0.26 ± 0.01	900 ± 70
LT8	0.06 ± 0.01	0.59 ± 0.03	0.30 ± 0.01	7.35	0.35 ± 0.02	20/16	0.04	CAM	0.30 ± 0.01	860 ± 60
LT9	0.05 ± 0.01	0.32 ± 0.02	0.22 ± 0.01	6.33	0.31 ± 0.02	20/19	0.11	CAM	0.32 ± 0.01	1,050 ± 75
LT10	0.07 ± 0.01	0.88 ± 0.03	0.30 ± 0.01	8.29	0.37 ± 0.02	20/15	0.11	CAM	0.38 ± 0.01	1,065 ± 60
LT11	0.05 ± 0.01	0.49 ± 0.02	0.39 ± 0.01	5.92	0.36 ± 0.02	20/17	0.07	CAM	0.41 ± 0.01	1,150 ± 70
LT12	0.06 ± 0.01	0.29 ± 0.01	0.34 ± 0.01	6.17	0.34 ± 0.02	20/19	0.12	CAM	0.42 ± 0.01	1,235 ± 80
LT13	0.06 ± 0.01	1.06 ± 0.03	0.69 ± 0.01	4.19	0.47 ± 0.02	20/17	0.02	CAM	0.79 ± 0.01	1,680 ± 75
LT14	0.06 ± 0.01	0.22 ± 0.01	0.24 ± 0.01	5.52	0.31 ± 0.02	20/16	0.10	CAM	0.50 ± 0.01	1,600 ± 110
LT15	0.05 ± 0.01	0.33 ± 0.02	0.19 ± 0.01	6.2	0.30 ± 0.02	20/17	0.06	CAM	0.43 ± 0.01	1,440 ± 105

4.2 Sedimentology of beach ridge plain at PTI

Five sedimentary logs derived from gouge cores were interpreted on site and are presented here as P1 to P5, with maximum depths ranging from approximately 70 to 90 cm. All cores were collected from swampy areas within large swales between beach ridges (Fig. 2d). At PTI, six main sedimentary units were identified: Unit A, Unit B (2004 IOT deposits), Unit C, Unit D, Unit X, and Unit E (Fig. 6). A summary of the characteristics of each unit is provided in Table 2. P1 preserves a 2004 tsunami-derived fine sand layer, approximately 11 cm thick, at the surface. Another potential paleo-tsunami layer, corresponding to Unit D, was identified at 23.5–31 cm depth. This layer consists of fine to medium sand interbedded with organic layers and exhibits an upward-fining trend. The lower organic soil of Unit C displays coarser grains toward the base, also showing an upward-fining trend. The beach basement, corresponding to Unit E, occurs below 75 cm depth and consists of medium to coarse sand with normal grading.

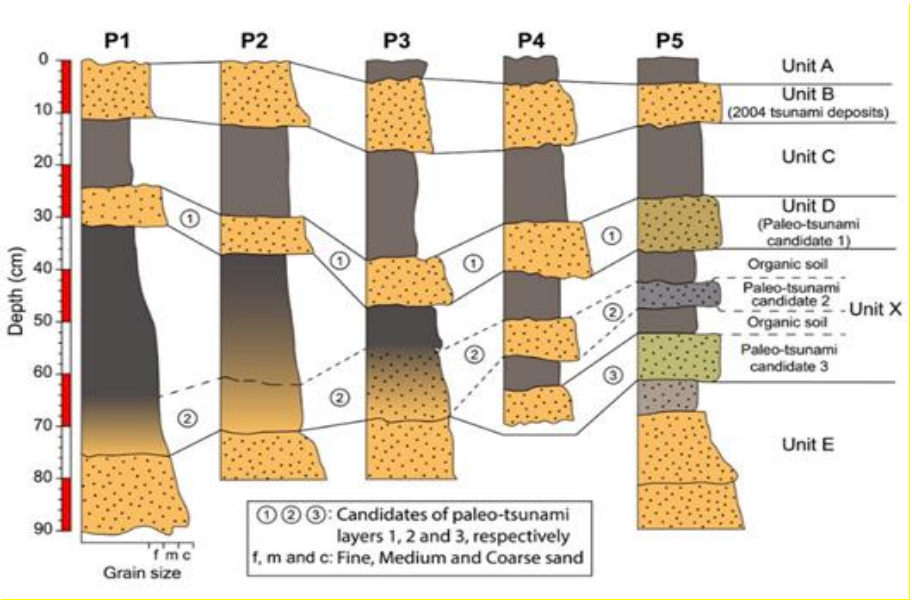

Figure 6: Stratigraphic correlation of detailed excavated pits along the outer swale of PTI. Three potential extreme wave sand sheets were comparatively inferred to paleo-tsunami sand sheets in Jankaew et al. (2008).

Across the same swale over a distance of 10 m, P2 was excavated. This pit contains two sand layers. The upper layer, corresponding to Unit B, represents the 2004 tsunami deposits at the surface, with a thickness of ~12 cm and normal grading. The lower layer, corresponding to Unit D, consists of fine to medium sand interbedded with organic layers and also exhibits normal grading. The beach basement, corresponding to Unit E, occurs below 70 cm depth and is composed of fine to coarse sand with normal grading. Both sand layers are interspersed with organic soils of Unit C.

P3, located approximately 10 m from Pit 2 along the long axis of the swale, preserves two candidate sand layers corresponding to Units B and D. The pit is covered by a thin topsoil layer (Unit A). The 2004 tsunami deposit (Unit B) occurs at 4–17 cm depth, with a thickness of ~13 cm. The second candidate paleo-tsunami layer (Unit D) is found at 38–47 cm depth, separated by organic-rich layers (Unit C). The characteristics of these layers are consistent with those observed in P1 and P2, consisting of fine to medium sand with normal grading. Below 55 cm, a mixed sand–organic layer (Unit X) develops, and the beach basement (Unit E) is encountered at approximately 70 cm depth.

P4, located 10 m from Pit 3 along the swale, contains up to four candidate paleo-tsunami layers. The pit is capped by a 5 cm thick topsoil (Unit A). The bioturbated 2004 tsunami deposit (Unit B) occurs at 5–18 cm depth, with a thickness of 13 cm. The second sand layer (Unit D) is present at 32–41 cm depth, beneath organic soils of Unit C. The third sand layer is located at 51–57 cm depth, interbedded with organic soils of Unit X, while the fourth candidate layer occurs below 63 cm depth. All four layers share similar characteristics, consisting of fine to medium sand with upward-fining trends and interdigitated with dark organic-rich soils.

P5, located approximately 20 cm from Pit 4, contains up to four candidate tsunami sand layers interbedded with organic soils of Units C and X. The 2004 tsunami deposit (Unit B) occurs at 5–13 cm depth, while the three additional candidate paleo-tsunami layers are found at 27–37 cm, 43–47 cm, and 52–62 cm within Unit X. All sand layers consist of fine to medium sand with normal grading, displaying colours ranging from grey-greenish brown, grey, to greyish green. Clayey sands begin forming below 62 cm, gradually transitioning to clayey coarse sands. The beach sand basement (Unit E) is encountered at ~82 cm depth and continues to the base of the core, consisting of clean, fine to coarse sands.

Table 2: Summary of sedimentological characteristics from cores collected at LI and PTI.

Unit	Cores	Description	Interpretation
A	LT1, P3, P4 and P5	Thin (< 5 cm thickness) black organic soils	Top soil
B	LT1, P1, P2, P3, P4 and P5	Fine to medium sand with normal grading, well sorted, low organic matters (<5%), carbonate contents (<1%)	2004 IOT deposits

C	P1, P2, P3, P4 and P5	Organic soils with roots	Swampy deposits
Upper C	LT1	Light color fine to very fine sand, well sorted, higher organic matters at top, very low carbonate percentages (near zero)	Low-energy swale deposits
Lower C	LT1	Light color fine to very fine sand, well sorted, steadily low organic matters, fluctuated high carbonate contents (0.60 – 6.62%)	Low-energy swale deposits with shell influx
D	LT1, P1, P2, P3, P4 and P5	Fine to medium sand with normal grading and small reverse grading at base in LT1, moderately well sorted, high carbonate contents (up to 12%), sharply changed in sedimentary parameters, 8-10 cm thick	Candidate 1 of paleo-tsunami deposits
X	P1, P2, P3, P4 and P5	Organic soils sharply contacted to one or two sand layers which are micaceous fine to medium sand with normal grading, grey to greyish green color and partly oxidized	Organic soil interspersed layers of paleo-tsunami sand candidates 2 and 3
E	LT1, P1, P2, P3, P4 and P5	Massive fine to coarse sand with normal grading, sub-angular shape, structureless	Beach deposits

5. DISCUSSIONS

5.1 Prehistoric beach ridge evolution along TMP

Ridge spacing, orientation, and sediment accumulation patterns suggest that coastal morphology was strongly influenced by the interplay of relative sea-level fluctuations, sediment availability, and episodic overwash events, highlighting the regional sensitivity of TMP coasts to Holocene sea-level dynamics. Average ridge progradation rates (~0.2 –1 mm yr^{-1}) further reflect the control of relative sea level regression on strand-plain growth. Integration of OSL chronology, sedimentology, and geomorphological mapping enables reconstruction of the Holocene evolution of the Andaman coast, demonstrating the role of extreme wave events in shaping beach ridge morphology and informing regional sea-level and sediment dynamics.

Monsoon intensity in the eastern Indian Ocean may have played an important role in controlling beach ridge progradation at LI and PTI. Seven discrete intervals of weakened summer monsoon activity during the Holocene, although small in amplitude, can be correlated (within radiocarbon age uncertainties) with millennial-scale cooling events in the North Atlantic, indicating synchronous monsoon weakening during cooler phases (Gupta et al., 2003). These findings suggest that even subtle interglacial variations in the North Atlantic, not only major glacial shifts, could significantly influence the Asian monsoon system. Similarly, after ~2 ka, $\delta^{18}O$ records from speleothems indicate reduced monsoon intensity and precipitation (Wang et al., 2005).

On the GoT side of the TMP, beach ridges formed during the middle to late Holocene. For example, Laem Pho at Chaiya district began forming at 7.2 ka and prograded eastward to the present during the middle to late Holocene (Polwichai et al., 2023). Chumphon ridges yield a maximum age of 8.9 ka in the middle Holocene (Nimnate et al., 2015), while Sathingpra Peninsula ridges range from 3.3 to 1.7 ka during the late Holocene (Laerosa et al., 2024). Along the Andaman coast, the western side of TMP, the Holocene sea-level history shows a mid-Holocene highstand locally up to +5 m between 7 and 5 ka, followed by a gradual fall or near-standstill through the late Holocene (Scheffers et al., 2012). PTI preserves beach ridges spanning 2.5 ka to A.D. 2004, with cross-shore progradation rates of 0.25–0.40 m yr^{-1} (Brill et al., 2015). Also, at PTI, sea-level fall of ~1.06 m between ~2660 and ~370 years ago, and between ~550 and ~350 years ago, indicates an accelerating decline in sea level (Kumar et al., 2024). Stratigraphical and sedimentological evidence indicates rapid seaward progradation of the LI beach ridge plain (~1,800 m) over approximately 1,680 years. Fifteen OSL ages from Transect 1 at LI show that the oldest preserved ridge sand in the northwestern area was deposited at 1.68 ± 0.08 ka, with seaward progradation continuing quasi-steadily to the present shoreline. The cross-shore distance between the innermost ridge (LT15) and the outermost ridge (LT1) is about 2,500 m, yielding a mean progradation rate of 1.07 m yr^{-1}. The faster progradation at LI compared to PTI likely reflects differences in sediment supply and may be related to variations in monsoon intensity.

5.2 Sedimentology of 2004 IOT as benchmark layers for ancient extreme wave records

The 2004 IOT deposits along the Andaman coast were extensively documented after the event (Hori et al., 2007; Umitsu et al., 2007; Choowong et al., 2007; Choowong et al., 2008a; Choowong et al., 2008b). The physical and chemical characteristics of tsunami deposits, however, vary spatially and depend on site-specific conditions, including sediment sources, flow dynamics, grain concentration in water, and local morphology. Among these properties, grain-size distribution serves as a key proxy for identifying

tsunami deposits along the Andaman coast (Choowong et al., 2008a; Choowong et al., 2008b; Jankaew et al., 2008; Fujino et al., 2008; Fujino et al., 2010; Goto et al., 2012; Fujino et al., 2016; Fujino et al., 2018; Matsumoto et al., 2023).

Grain sizes of tsunami deposits reported in previous studies range from fine to coarse sand. At Phuket, the 2004 IOT deposits consist of medium to coarse sand with a mean grain size of 0–2 φ (Choowong et al., 2008b; Jankaew et al., 2008). In this study at LI, the Unit B deposits are presented as a thin layer (~24 cm thick), well sorted ($\sigma \approx 0.46$ φ), and with low carbonate content (<0.3 wt%). These characteristics are consistent with typical tsunami signatures reported at Bangtao beach, Phuket (Choowong et al., 2008b), including single sand sheets, normally graded, very well sorted, rarely exceeding 30 cm in thickness, and containing minimal carbonates. Generally, 2004 IOT deposits at LI are predominantly fine sands (2.90 φ–3.00 φ), whereas at PTI deposits are slightly coarser, ranging from fine to medium sands. This difference likely reflects variations in local sediment sources and topography. The geological setting of LT consists of Carboniferous–Permian fine-grained clastic sedimentary rocks, with main sediment sources being claystone, argillaceous sandstone, and siltstone. Moreover, LI is located in the lee of the Sumatra Islands and is partially sheltered by small surrounding islands, which likely reduced the energy of tsunami waves. Consequently, fine sands were delivered and deposited as the 2004 IOT sand sheet of Unit B at LI (Fig. 6).

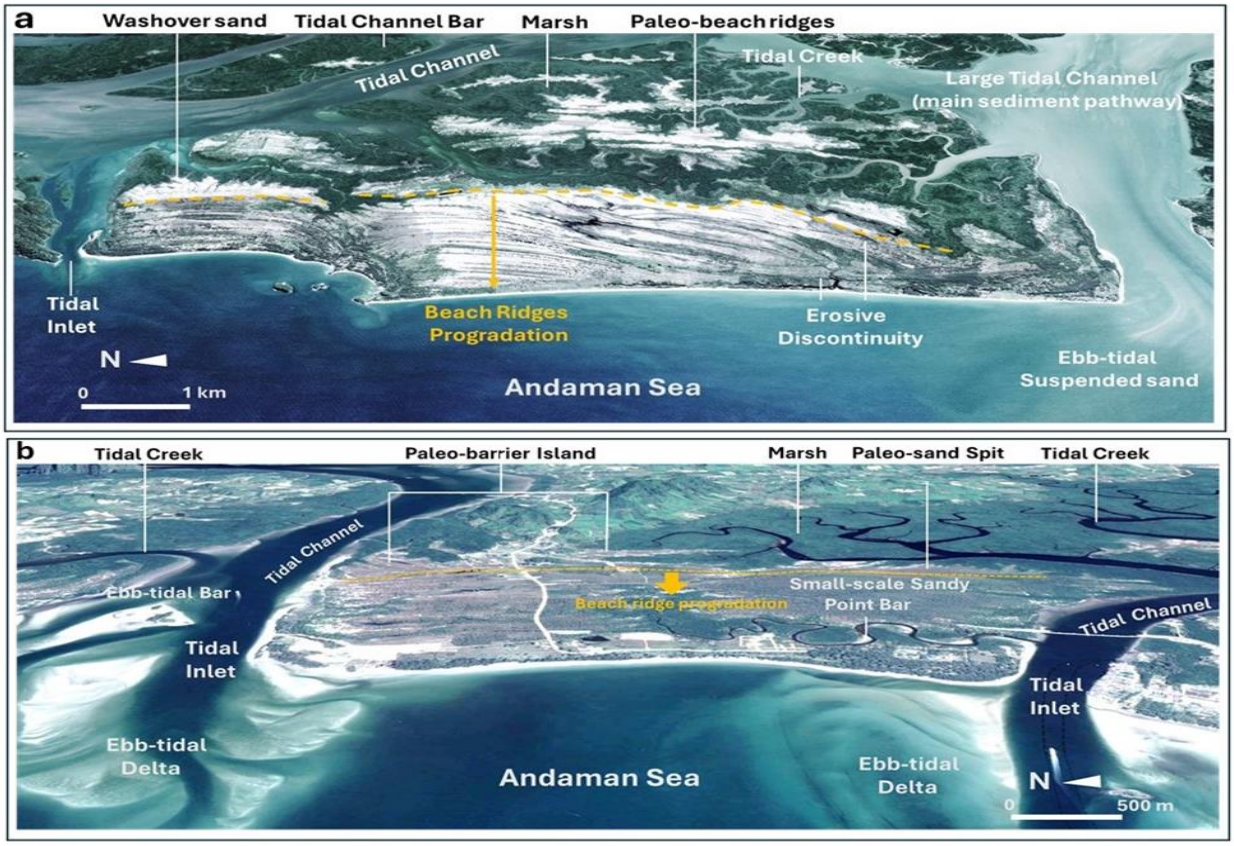

Figure 7: Satellite images from Google Earth taken in January 2017. (a) Beach ridges progradation at PTI with associated morphological landforms in comparison to LI (b).

The depth of swales at both LI and PTI ranges from 0.5 to 1 m. The deepest swale at LI formed roughly 800–900 years ago, about 950 m from the present shoreline, corresponding well with the large swales developed at PTI (Brill et al., 2015). These findings confirm that the late Holocene strand-plain development was primarily controlled by relative sea-level fall or near-standstill conditions. However, progradation at LI continued between 1,000 and 2,000 years ago across a distance of 1,000–1,500 m, contrasting with PTI, where beach erosion occurred during the same period. Although both LI and PTI exhibit westward progradation of beach-ridge plains, the rate of progradation at LI during the late Holocene is approximately twice that of PTI. This clearly reflects a difference in sediment supply.

Considering the morphology of both islands, which include tidal channels in the north and south, the tidal channels at LI are larger than those at PTI. This likely enhanced the inland sediment transport toward the river mouth, forming a more extensive ebb-tidal delta (Fig. 7). Inner beach ridges preserved landward of the tidal channel at PTI were dated to around 100 ka in the Pleistocene (Brill et al., 2015) and are described as paleo–beach ridges. Seaward of this tidal channel, the morphology of washover sands appears to remain preserved behind a set of prograding beaches (Fig. 7a). At PTI, Brill et al. (2015) interpreted several straight-line features as erosional discontinuities. Comparable erosional patterns were not clearly observed at LI (Fig. 7b). Nonetheless, some straight lines cutting across beach ridges and swales at PTI might be possibly related to extensive tin-mining activities in recent decades. When river input is the dominant source of coastal sediments, the volume of sediment accumulating along the shoreline tends to correspond to the river's sediment discharge, which is itself influenced by precipitation patterns driven by climate change (Tamura, 2012).

5.3 Candidate layers and age of extreme waves

Successive sand sheets and grain-size variations indicate episodic high-energy deposition events, likely representing tsunamis or storms. Distinctive high-energy layers in core LT1, characterized by peaks in grain size, sorting, skewness, and kurtosis, correspond to paleo-tsunami or storm events. Comparison with modern 2004 IOT deposits confirm these layers as reliable chronological markers, providing evidence of episodic extreme wave activity punctuating otherwise gradual Holocene sedimentation. Previous studies at PTI and Ban Bang Sak, Phang-nga, Thailand, have documented storm-washover fans deposited by the 2007 and earlier cyclones, forming lobate, landward-thinning packages with multiple scour-and-fill couplets and minimal upward grading (Choowong et al., 2009; Phantuwongraj and Choowong, 2012; Gouramanis et al., 2017; Kumar et al., 2024). Such architecture is observed in the top of LI core at 4-12 cm (Fig. 5). In comparison with the well-defined tsunami deposits at PTI: the 2004 IOT sheet (Unit B) was found at 8–32 cm. However, PTI preserves up to four candidate tsunami layers, including the 2004 IOT sand sheet (Unit B), one Unit D layer, and one to two candidate sand sheets of Unit X (Fig. 6). Several lines of evidence support the interpretation of these layers as tsunami deposits rather than storm deposits. First, their sedimentological characteristics differ from storm-washover deposits. Sorting remains well maintained ($\sigma \leq 0.9\ \varphi$), carbonate and organic spikes coincide with single, sharp-based beds rather than stacked cosets, and skewness returns to positive values immediately below the paleo-tsunami sheets, whereas storm sequences typically exhibit repeated oscillations across all grain-size moments. Second, geographical position of LI limits the exposure to extreme waves. LI is located in the east of Phi Phi Island, which filters almost cyclone surges, whereas tsunamis, with longer wavelengths and higher run-up, can still overtop the beach-ridge plain. This also likely explains why the number of candidate storm and tsunami layers at LI is fewer than at PTI.

Three sand sheets at PTI, sharply bounded by organic sands or soils, were interpreted as candidate tsunami deposits (Fig. 6), inferred by comparison with well-studied PTI sites (Jankaew et al., 2008; Prendergast et al., 2012). Their sedimentological parameters—including grain size, sorting, skewness, kurtosis, and carbonate content—are notably consistent with tsunami deposits. Prendergast et al. (2012) reported OSL ages for three sand sheets at PTI, from top to bottom, likely deposited by tsunamis of comparable magnitude to the 2004 IOT, with ages of 380 ± 50, 990 ± 130–1410 ± 190, and 2100 ± 260 years before AD 1950. The youngest of these aligns with previous radiocarbon-based estimates by Jankaew et al. (2008), suggesting that the most recent large-scale predecessor to the 2004 IOT occurred shortly after 550–700 cal BP.

5.4 Prehistoric to medieval sea level changes

Based on OSL-derived ages from LI and comparative regional data, we propose an updated sea-level curve for the western TMP. The curve indicates a mid-Holocene highstand (+1–2.5 m, locally +5 m) between 7–5 ka, followed by gradual fall or near-standstill through the late Holocene. Late Holocene ridge formation at LI and PTI supports a period of relatively stable sea level, allowing continuous strand-plain progradation, with regional differences reflecting variations in sediment supply and local geomorphology. This updated reconstruction used OSL dating resulted from this work and previous studies provides a robust framework for understanding coastal evolution and beach ridge development (Fig. 8). Ages derived from beach ridges (Scheffers et al., 2012; Kongsen et al., 2022; Kumar et al., 2024), corals and oysters (Scheffers et al., 2012) in the west TMP correspond to the glacial isostatic adjustment models (GIA) at Phuket (Horton et al., 2005). The general pattern of the late Holocene sea-level curve from the TMP is similar to those from the GoT.

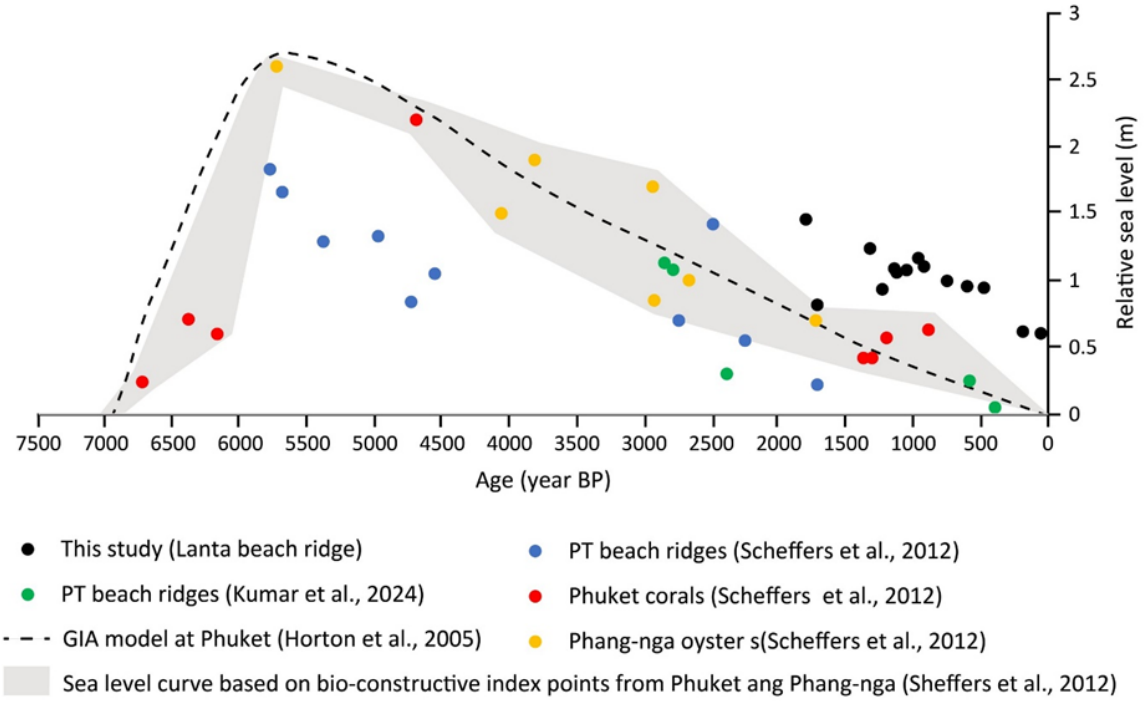

Figure 8: Updated sea-level curves. All curves proposed for the western TMP based on OSL and radiocarbon datings.

5.5 Sea-level changes interface to archaeology

In the TMP, Neolithic developments since the mid-Holocene, have been documented primarily through archaeological evidence (Bellina et al., 2019; Ploymukda, 2019; Rotchanarat, 2019). However, the relationships between physical processes particularly sea-level fluctuations and coastal lifeways during periods when sea level stood approximately 1.5-3.0 m above the present mean sea level (MSL) have received little attention. On adjacent islands of LI (Fig. 9), rock paintings preserved on limestone cliffs have been identified (Srisuchat, 1987; Bellina et al., 2021). The largest sailboat painting (1.6 m in height) on the limestone cliff wall at Ko Ra Pa Phang is situated between 3.1 m (measured at the base of the painting) and 4.7 m above the present MSL (Fig. 10). Based on its elevation, the painting likely predates the formation of the beach-ridge plain at LI, which developed after ca. 1,800 years BP, when sea level was approximately 1.8 m above the present MSL. This suggests that the sailboat motif was created when sea level was at least ~1.3 m higher than present. In addition to paintings on cave walls and within sea notches, several motifs depicting fish and human figures were recorded at elevations of approximately 4–5 m above the present MSL. These paintings are tentatively interpreted as belonging to the prehistoric period, dating to around 3,000 years BP (Rotchanarat et al., 2024), corresponding to regional sea-level records that indicate sea levels of approximately 2 m above present.

Archaeological evidence further suggests long-term human occupation and maritime resource use in this region, extending from the prehistoric period to historical times. Alongside the TMP, prehistoric archaeological sites are inferred to have existed prior to the formation of the beach-ridge plain on LI, indicating that human settlement and coastal evolutional practices predate late-Holocene shoreline progradation. This continuity of occupation and maritime engagement persisted into the historical period, during which archaeological evidence points to the integration of the Andaman Sea coast into broader maritime exchange systems, possibly including routes associated with the Maritime Silk Roads (e.g., Sanghiran, 2019). These networks facilitated connections between the Andaman coast of the TMP and the GoT, highlighting the role of this coastal zone as a long-standing corridor of human movement, seafaring, and cultural interaction.

Throughout the extended period represented by archaeological evidence—from before the formation

of the LI beach-ridge plain through to the historical era—geological records indicate that the region experienced multiple high-energy marine events, including tsunamis and severe storm surges. These events provide clear evidence that coastal communities in this area were repeatedly exposed to large-scale marine hazards. The persistence of coastal settlement, fishing lifeways, and sustained maritime connectivity despite such recurrent hazards highlights a remarkable degree of human adaptation to dynamic and hazardous coastal environments. Continuous engagement with the sea, both for subsistence and for interregional travel, reflects adaptive strategies that enabled long-term coexistence with natural processes, offering important insights into past human resilience within changing coastal landscapes.

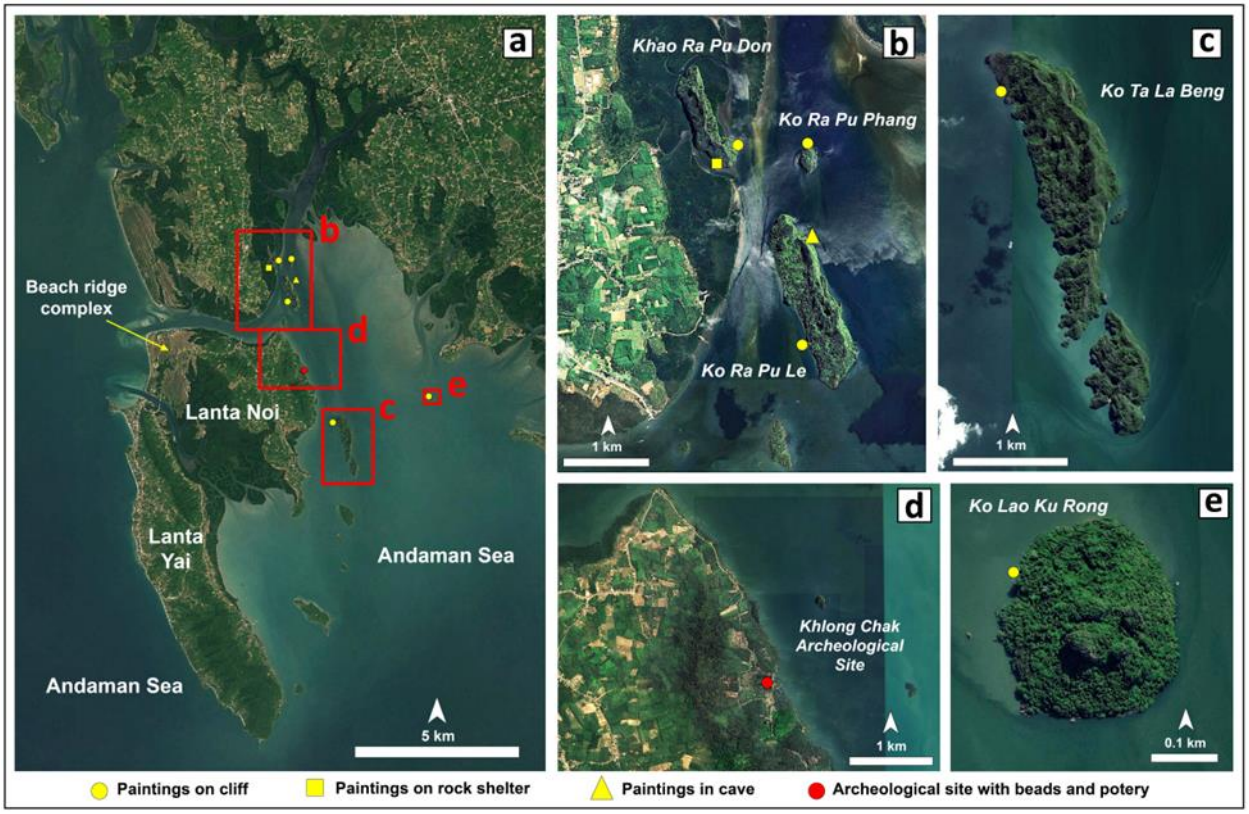

Figure 9: Locations of prehistoric paintings and archaeological site. (a) Lanta islands and nearby archipelago in Krabi province. (b) Khao Ra Pu Don, Ko Ra Pu Phang and Ko Ra Pu Le islands. (c) Ko Ta La Beng island. (d) Khlong Chak archaeological site and (e) Ko Lao Ku Rong Island.

Motifs depicting fish and watercraft can be interpreted as reflecting subsistence practices cantered on fishing and seafaring activities of prehistoric coastal populations. The representation of sailing boats (Figs. 10 to 12), in particular, may indicate regular offshore navigation and the existence of established maritime routes. The height of the paintings relative to the present mean sea level suggests that they may have been created under higher sea-level conditions, potentially from boats or floating platforms, when access to the cliff faces was facilitated by elevated water levels. The location of these paintings on prominent limestone cliffs facing the sea raises the possibility that the islands functioned not only as habitation or ritual spaces, but also as navigational landmarks or waypoints along coastal and inter-island travel routes. Such visual markers may have played an important role in wayfinding, reinforcing collective knowledge of seascapes and movement corridors during a period of higher relative sea level. This interpretation highlights the potential of rock art as an integrated record of maritime lifeways, navigation practices, and human adaptation to mid- to late-Holocene coastal environments.

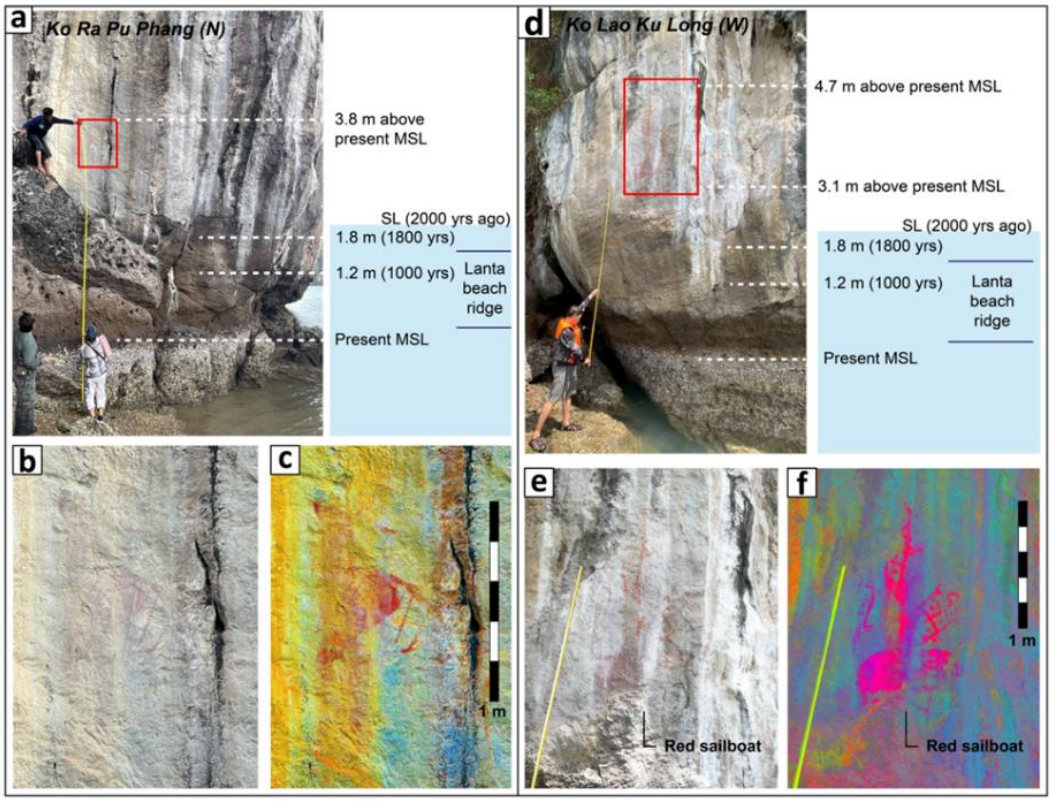

Figure 10: Positions of rock paintings on limestone cliff comparison with sea level from prehistoric to medieval periods. (a) Sailboat with dimension 1.6 m height and fish painted at 3.1 m above present MSL, (b) close-up picture and (c) color enhance technique. (d) Another sailboat painted on cliff wall at 3.5-3.8 m above present MSL, with close-up picture and color enhance (e and f).

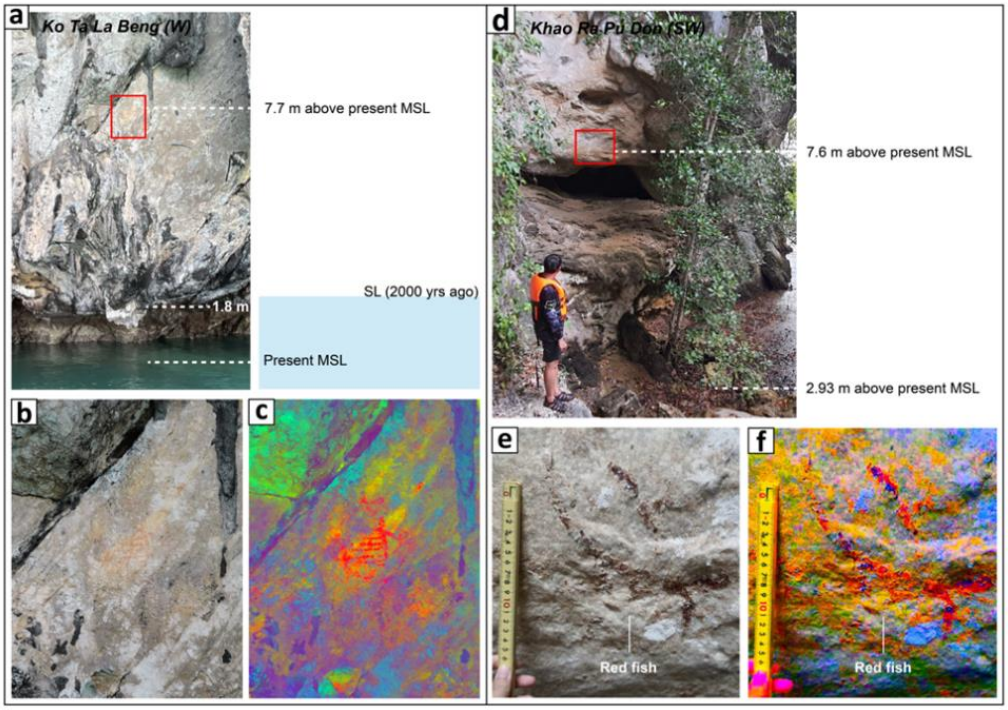

Figure 11: (a) Cliff on western part of Ko Ta La Beng with prehistoric paints (b) and compared paint after rock art enhancer adjustment (c). Rock shelter on south-western part of Khao Ra Pu Don (d) with prehistoric fish paints (e) and compared paint after rock art enhancer adjustment (f).

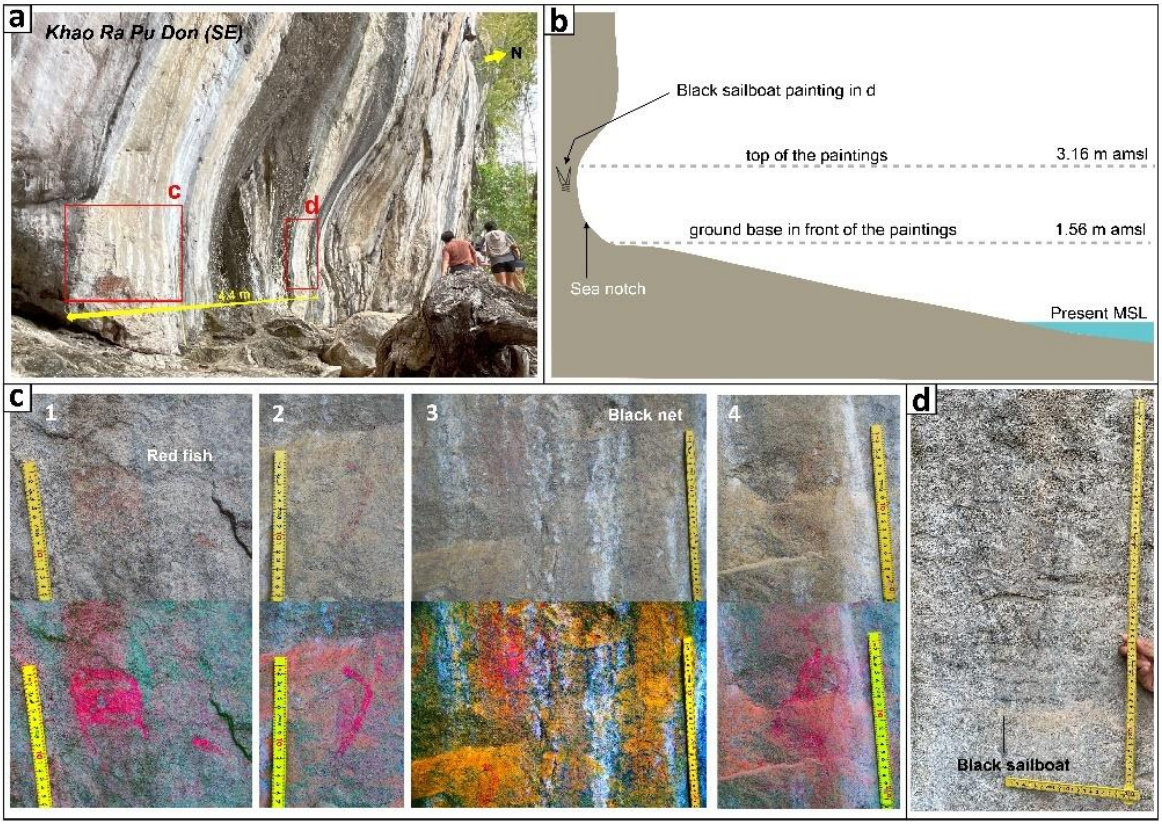

Figure 12: (a) Sea notch on the south-eastern part of Khao Ra Pu Don with two groups of prehistoric paints. (b) Model of the site relative to present sea level. (c) Groups of paints including fish (C1), unidentified pattern (C2 and C4) and black net (C3) on the upper row compared with the paints after rock art enhancer adjustment on the bottom row.

6. CONCLUSION

The coastal landscapes of the Andaman coast of the TMP demonstrate that sea-level change and extreme coastal hazards have been recurring forces shaping both the physical environment and human activity over millennia. Beach ridge–swale systems preserve stratigraphic records of tsunamis and severe storms, while associated archaeological evidence—including prehistoric rock paintings—reveals long-term human adaptation to coastal instability. These combined records show that extreme waves are not anomalous events but part of a repeating coastal history that has influenced settlement patterns, mobility, and perhaps the local maritime networks.

From a policy perspective, integrating geomorphological and archaeological archives into coastal risk assessments offers a longer-term context than instrumental and historical records alone. The identification of multiple extreme wave events predating the 2004 IOT highlights the need to reconsider hazard recurrence intervals and to incorporate deep-time evidence into disaster risk reduction and coastal planning strategies. Beach ridge plains, particularly their swales, should be recognized as key geomorphological and cultural archives that warrant protection within coastal management frameworks.

Furthermore, prehistoric rock art sites and archaeological materials located within present-day marine and coastal zones are highly vulnerable to ongoing sea-level rise, coastal erosion, and development pressures. These sites represent irreplaceable prehistorical heritage and should be explicitly included in coastal risk zoning, heritage impact assessments, and climate adaptation policies. By bridging sedimentological evidence with archaeology and cultural landscapes, this study emphasizes that effective coastal policy must address not only physical risk but also the preservation of maritime heritage. Recognizing how past societies lived with the sea can inform more resilient, culturally sensitive approaches to managing future coastal change along the Andaman coast.

Author Contributions: Stapana Kongsen: Conceptualization, formal analysis, writing the first draft of manuscript, investigation, visualization. Chanakan Ketthong: Conceptualization, investigation, writing, visualization. Sirawat Udomsak: Investigation. Chanista Chansom: Investigation. Peerasit Surakiatchai: Investigation. Patcharaporn Ngernkerd: Investigation and archaeology analysis. Nutcha Choowong: Editing, GIS and maps. Norakrit Butkaew, Peerasak Klubket: Investigation. Sumet Phantuwongraj Santi Pailoplee, Akkaneewut Jirapinyakul, Kantapon Suraprasit and Vichai Chutakositkanon: Essentially intellectual contributions. Montri Choowong: Conceptualization, formal analysis, writing, editing, funding acquisition.

Acknowledgements: SK is supported by the Second Century Fund (C2F), Chulalongkorn University through a post-doctoral scholarship. Research Affairs Office and the Faculty of Science, Chulalongkorn University sponsored MC to attend the GEST 2024 conference. This work was partially funded by the Fundamental Fund 69 program (DIS_FF_69_113_2300_030), Chulalongkorn University, and the Thailand Science Research and Innovation (TSRI). Special thanks are extended to Prof. Dr. Frank Preusser, Alexander Fulling, and Jenny Wolff from the University of Freiburg for their support in OSL dating, grain-size analyses, and De sample preparation and measurements. The MESA Center of Excellence, Department of Geology, Chulalongkorn University, is acknowledged for logistical support and laboratory facilities. Thanks also to Dr. Yuki Sawai, the editor and reviewers for the comments that strengthened the quality of manuscript.

REFERENCES

Atwater, B.F., Musumi-Rokkaku, S., Satake, K., Tsuji, Y., Ueda, K., and Yamaguchi, D.K. (2005) The orphan tsunami of 1700—Japanese clues to a parent earthquake in North America, 1st Edition: Seattle, University of Washington Press, U.S. Geological Survey Professional Paper 1707, 135 p.

Bellina, B., Favereau, A., Dussubieu, L. (2019) Southeast Asian early Maritime Silk Road trading polities' hinterland and the sea-nomads of the Isthmus of Kra. Journal of Anthropological Archaeology, Vol. 54, 102–120

Bellina, B., Rotchanarat, S., Tan, N.H., Évrard, O.E. (2021) Coastal heritage: Exploring caves and indigenous knowledge in the Lanta Bay (southern Thailand). Journal of Indo-Pacific Archaeology, Vol. 45 (2021), 25–41

Bell, W.T. (1979) Attenuation factors for the absorbed radiation dose in quartz inclusion for Thermoluminescence dating. Ancient TL, Vol. 8, 2-13. https://DOI: 10.26034/la.atl.1979.022

Brill, D., Jankaew, K., Brückner, H. (2015) Holocene evolution of Phra Thong's beach-ridge plain (Thailand) — Chronology, processes and driving factors. Geomorphology, Vol. 245, 117–134. https://doi.org /10.1016/j.geomorph.2015.05.016

Brill, D., Klasen, N., Jankaew, K., Brückner, H., Kelletat, D., Scheffers, A., Scheffers, S. (2012) Local inundation distances and regional tsunami recurrence in the Indian Ocean inferred from luminescence dating of sandy deposits in Thailand. Natural Hazards and Earth System Science., Vol. 12 (7), 2177–2192. https://doi.org/10.5194/nhess-12-2177-2012

Chlieh, M., Avouac, J.-P., Hjörleifsdóttir, V., Song, T.-R., Ji, C., Sieh, K., Sladen, A., Hébert, H., Prawirodirdjo, L., Bock, Y., Galetzka, J. (2007) Coseismic slip and afterslip of the great Mw 9.15 Sumatra–Andaman earthquake of 2004. Bulletin of Seismological Society of America, Vol. 97, S152–S173. https:// doi.org/10.1785/0120060616

Choowong, M. (2011) "Quaternary", Book Series "Geology of Thailand". In: Ridd, M.F., Barber, A.J., Crow, M.J. (Eds). Geological Society of London (Chapter 12), 335-350

Choowong, M., Murakoshi, N., Hisada, K., Charusiri, P., Daorerk, V., Charoentitirat, T., Chutakositkanon, V., Jankaew, K., Kanjanapayont, P. (2007) Erosion and deposition by the 2004 Indian Ocean tsunami in Phuket and Phang-nga Provinces, Thailand. Journal of Coastal Research, Vol. 23(5), 1299–1313. https://doi.org/10.2112/06-0922.1

Choowong, M., Murakoshi, N., Hisada, K.-i., Charoentitirat, T., Charusiri, P., Phantuwongraj, S., Wongkok, P., Choowong, A., Subsayjun, R., Chutakositkanon, V., Jankaew, K., Kanjanapayont, P. (2008a) Flow conditions of the 2004 Indian Ocean tsunami in Thailand, inferred from capping bedforms and sedimentary structures. Terra Nova, Vol. 20(2), 141–149. https://doi.org/10.1111/j.1365-3121.2008.00786.x

Choowong, M., Murakoshi, N., Hisada, K.-i., Charusiri, P., Charoentitirat, T., Chutakositkanon, V., Jankaew,

K., Kanjanapayont, P., Phantuwongraj, S. (2008b) 2004 Indian Ocean tsunami inflow and outflow at Phuket, Thailand. Marine Geology, Vol. 248(3–4), 179–192. https://doi.org/10.1016/j.margeo.2007.12.006

Choowong, M., Phantuwongraj, S., Charoentitirat, T., Chutakositkanon, V., Yumuang, S., Charusiri, P. (2009) Beach recovery after 2004 Indian Ocean tsunami from Phang-nga, Thailand. Geomorphology, Vol. 104(3–4), 134–142. https://doi.org/10.1016/j.geomorph.2008.10.011

Feldens, P., Schwarzer, K., Szczuciński, W., Stattegger, K., Sakuna, D., Sompongchaiyakul, P. (2009) Impact of 2004 tsunami on seafloor morphology and offshore sediments, Pakarang Cape, Thailand. Polish Journal of Environmental Studies, Vol. 18, 63–68.

Fujino, S., Goto, K., Tappin, D., Fujiwara, O. (2016) Geological records of storms, tsunamis and other extreme events. Island Arc, Vol. 25(5), 303–304. https://doi.org/10.1111/iar.12137

Fujino, S., Kimura, H., Komatsubara, J., Matsumoto, D., Namegaya, Y., Sawai, Y., Shishikura, M. (2018) Stratigraphic evidence of historical and prehistoric tsunamis on the Pacific coast of central Japan: Implications for the variable recurrence of tsunamis in the Nankai Trough. Quaternary Science Reviews, Vol. 201, 147–161. https://doi.org/10.1016/j.quascirev.2018.09.018

Fujino, S., Naruse, H., Matsumoto, D., Jarupongsakul, T., Sphawajruksakul, A., Sakakura, N. (2009) Stratigraphic evidence for pre-2004 tsunamis in southwestern Thailand. Marine Geology, Vol. 262(1–4), 25–28. https://doi.org/10.1016/j.margeo.2009.01.002

Fujino, S., Naruse, H., Matsumoto, D., Sakakura, N., Suphawajruksakul, A., Jarupongsakul, T. (2010) Detailed measurements of thickness and grain size of a widespread onshore tsunami deposit in Phang-nga Province, southwestern Thailand. Island Arc, Vol. 19(3), 389–398. https://doi.org/10.1111/j.1440-1738.2010.00718.x

Fujino, S., Naruse, H., Suphawajruksakul, A., Jarupongsakul, T., Murayama, M., Ichihara, T. (2008) Thickness and grain-size distribution of Indian Ocean tsunami deposits at Khao Lak and Phra Thong Island, South-Western Thailand. In: Tsunamites, pp. 123–132.

Goto, K., Takahashi, J., Fujino, S. (2012) Variations in the 2004 Indian Ocean tsunami deposits thickness and their preservation potential, southwestern Thailand. Earth, Planets and Space, Vol. 64(10), 923–930. https://doi.org/10.5047/eps.2012.05.002

Gouramanis, C., Switzer, A.D., Jankaew, K., Bristow, C.S., Pham, D.T., Ildefonso, S.R. (2017) High-frequency coastal overwash deposits from Phra Thong Island, Thailand. Scientific Reports, Vol. 7, 43742. https://doi.org/10.1038/srep43742

Gouramanis, C., Switzer, A.D., Pham, D.T., Rubin, C., Lee, Y.S., Bristow, C., Jankaew, K. (2014) Thin-bed ground-penetrating radar analysis of preserved modern and palaeotsunami deposits from Phra Thong Island, Thailand. In: Proceedings of the 15th International Conference on Ground Penetrating Radar, 1017–1022.

Gouramanis, C., Switzer, A.D., Polivka, P.M., Bristow, C.S., Jankaew, K., Dat, P.T., Pile, J., Rubin, C.M., Yingsin, L., Ildefonso, S.R., Jol, H.M. (2015) Ground penetrating radar examination of thin tsunami beds — A case study from Phra Thong Island, Thailand. Sedimentary Geology, Vol. 329, 149–165. https://doi.org/10.1016/j.sedgeo.2015.05.006

Gouramanis, C., Yan, Y.T., Yang, Z., Soria, J.L., Yap, A., Jankaew, K., Switzer, A.D. (2025) Storm sediment deposit from Ko Phra Thong, Thailand. Marine Geology, Vol. 489, 107641. https://doi.org/10.1016/j.margeo.2025.107641

Gupta, A., Anderson, D., Overpeck, J. (2003) Abrupt changes in the Asian southwest monsoon during the Holocene and their links to the North Atlantic Ocean. Nature, Vol. 421, 354–357. https://doi:10.1038/nature01340.

Hawkes, A.D., Bird, M., Cowie, S., Grundy-Warr, C., Horton, B.P., Shau Hwai, A.T., Law, L., Macgregor, C., Nott, J., Ong, J.E., Rigg, J., Robinson, R., Tan-Mullins, M., Sa, T.T., Yasin, Z., Aik, L.W. (2007) Sediments deposited by the 2004 Indian Ocean tsunami along the Malaysia–Thailand Peninsula. Marine Geology, Vol. 242(1–3), 169–190. https://doi.org/10.1016/j.margeo.2007.02.006

Heiri, O., Lotter, A.F., Lemcke, G. (2001) Loss on ignition as a method for estimating organic and carbonate content in sediments: reproducibility and comparability of results. Journal of Paleolimnology, Vol. 25, 101-110. https://doi.org/10.1023/A:1008119611481

Hori, K., Kuzumoto, R., Hirouchi, D., Umitsu, M., Janjirawuttikul, N., Patanakanog, B. (2007) Horizontal and vertical variation of 2004 Indian tsunami deposits: An example of two transects along the western coast

of Thailand. Marine Geology, Vol. 239, 163-172. https://doi.org/10.1016/j.margeo.2007.01.005

Horton, B., Gibbard, P.L., Milne, G.M., Morley, R.J., Purintavaragul, C., Stargardt, J.M. (2005) Holocene sea levels and palaeoenvironments, Malay–Thai Peninsula, southeast Asia. The Holocene, Vol. 15, 1199–1213. https://doi.org/10.1191/0959683605hl891rp

Jankaew, K., Atwater, B.F., Sawai, Y., Choowong, M., Charoentitirat, T., Martin, M.E., Prendergast, A. (2008) Medieval forewarning of the 2004 Indian Ocean tsunami in Thailand. Nature, Vol. 455(7217), 1228–1231. https://doi.org/10.1038/nature07373

Kongsen, S., Phantuwongraj, S., Choowong, M., Chawchai, S., Udomsak, S., Chansom, C., Ketthong, C., Surakiatchai, P., Miocic, M.J., Preusser, F. (2022) Multi-proxy approach to identify the origin of high energy coastal deposits from Laem Son National Park, Andaman Sea of Thailand. Quaternary International, Vol. 625, 82-95 https://doi.org/10.1016/j.quaint.2022.04.017

Kumar, R., Switzer, A.D., Gouramanis, C., Bristow, C.S., Shaw, T.A., Jankaew, K., Li, T., Brill, D. (2024) Late-Holocene sea-level markers preserved in a beach ridge system on Phra Thong Island, Thailand. Geomorphology, Vol. 465, 109405. https://doi.org/10.1016/j.geomorph.2024.109405

Laerosa, A., Pradit, S., Wattanavatee, K., Dürrast, H., Vichaidid, T., Luengchavanon, M., Noppradit, P. (2024) Coastal evolution of Satingpra Peninsula, Songkhla Province: Implications for understanding Songkla Lagoon formation. Trends in Sciences, Vol. 21, 7508.

Lansai, C. (2004) Evolution of the Phrathong Island, Phang-nga, southern Thailand. B.Sc. Thesis, Department of Geology, Faculty of Science, Chulalongkorn University.

Lay, T., Kanamori, H., Ammon, C.J., Nettles, M., Ward, S.N., Aster, R.C., Beck, A.L., Bilek, S.L., Brudzinski, M.R., Butler, R., Deshon, H.R., Ekström, G., Satake, K., Sipkin, S. (2005) The Great Sumatra–Andaman Earthquake of 26 December 2004. Science, Vol. 308, 1127–1133. https://doi: 10.1126/science.1112250.

Naruse, H., Fujino, S., Suphawajruksakul, A., Jarupongsakul, T. (2010) Features and formation processes of multiple deposition layers from the 2004 Indian Ocean tsunami at Ban Nam Kem, southern Thailand. Island Arc, Vol. 19(3), 399–411. https://doi.org/10.1111/j.1440-1738.2010.00719.x

Nimnate, P., Chutakositkanon, V., Choowong, M., Pailoplee, S., Phantuwongraj, S. (2015) Evidence of Holocene sea level regression from Chumphon coast of the Gulf of Thailand. ScienceAsia, Vol. 41, 55–63. https://doi.org/10.2306/scienceasia1513-1874.2015.41.055

Matsumoto, D., Sawai, Y., Tanigawa, K., Namegaya, Y., Shishikura, M., Kagohara, K., Fujiwara, O., Shinozaki, T. (2023) Sedimentary diversity of the 2011 Tohoku-oki tsunami deposits on the Sendai coastal plain and the northern coast of Fukushima Prefecture, Japan. Progress in Earth Planet Sciences., Vol. 10, 23. https://doi.org/10.1186/s40645-023-00553-3

Prendergast, A.L., Cupper, M.L., Jankaew, K., Sawai, Y. (2012) Indian Ocean tsunami recurrence from optical dating of tsunami sand sheets in Thailand. Marine Geology, 297–298, 20–27. https://doi.org/10.1016/j.margeo.2011.12.003

Phantuwongraj, S., Choowong, M. (2012) Tsunami versus storm deposits from Thailand. Natural Hazards, Vol. 63, 31–50. https://doi.org/10.1007/s11069-011-0028-4

Ploymukda, S. (2019) Shipwreck of the Ancient Trans – Oceanic Trades from the Andaman Sea to the Gulf of Thailand. Ancient Maritime Cross-cultural Exchanges Archaeological Research in Thailand. The Fine Arts Department, Ministry of Culture. 248-263.

Polwichai, S., Phantuwongraj, S., Choowong, M. (2023) Beach ridge evolution in response to the Holocene sea-level change from Surat Thani, Thai-Malay Peninsula. ScienceAsia, Vol. 49, 353–360. https://doi.org/10.2306/scienceasia1513-1874.2023.49.353

Preusser, F., Degering, D., Fuchs, M., Hilgers, A., Kadereit, A., Klasen, N., Krbetschek, M., Richter, D., Spencer, J.Q.G. (2008) Luminescence dating: basics, methods and applications. Eiszeitalter und Gegenwart Quaternary Science Journal, Vol. 51(1-2), 95-149.

Rotchanarat, S. (2019) The Past and Present of Sea People; A Link between Prehistoric Pictographs and Ritual Performance of the Chao Le. Ancient Maritime Cross-cultural Exchanges Archaeological Research in Thailand. The Fine Arts Department, Ministry of Culture. 264-285.

Rotchanarat, S., Tan, N.H., Bellina, B., Evrard, O., Bowonsachoti, J. (2024) Maritime landscape and rock art traditions at Lanta Bay, Krabi, Thailand. From Megaliths to Maritime Landscapes: Perspectives on Indo-Pacific Archaeology, 130-144.

Sanghiran, S. (2019) Archaeological Sites and Findings on the Lower Peninsula of Thailand from the Seventh to Thirteenth Century Reflecting the Maritime Silk Road. Ancient Maritime Cross-cultural Exchanges

Archaeological Research in Thailand. The Fine Arts Department, Ministry of Culture. 54-77.

Satake, K., Aung, T., Sawai, Y., Okamura, Y., Win, K., Swe, W., Swe, C., Tint, L., Swe, T., Tun, S.T., Soe, M., Oo, T., Zaw, S. (2006) Tsunami heights and damage along the Myanmar coast from the December 2004 Sumatra-Andaman earthquake. Earth, Planets and Space, Vol. 58, 243–252. https://doi.org /10.1186/BF03351914

Sawai, Y., Jankaew, K., Martin, M.E., Prendergast, A.L., Choowong, M., Charoentitirat, T. (2009) Diatom assemblages in tsunami deposits associated with the 2004 Indian Ocean tsunami at Phra Thong Island, Thailand. Marine Micropaleontology, Vol. 73, 70–79. https://doi.org/10.1016/j.marmicro.2009.07.003

Scoffin TP and le Tissier MDA. (1998) Late Holocene sea level and reef flat progradation, Phuket, South Thailand. Coral Reefs, Vol. 17, 273–276. https://doi.org/10.1007/s003380050128

Scheffers, A., Brill, D., Kelletat, D., Brückner, H., Scheffers, S., Fox, K. (2012) Holocene Sea levels along the Andaman Sea coast of Thailand. The Holocene, Vol. 22, 1169–1180. http://DOI: 10.1177/ 0959683612441803

Srisuchat, A. (1987) Prehistoric cave and some important prehistoric sites in southern Thailand. In Final Report of the Seminar in Prehistory of Southeast Asia, Bangkok: SPAFA Co-ordinating Unit. pp. 103–117.

Stein, S., Okal, E.A. (2007) Ultralong period seismic study of the December 2004 Indian Ocean earthquake and implications for regional tectonics and the subduction process. Bulletin of Seismological Society of America, Vol. 97, S279–S295. https://doi.org/10.1785/0120060610

Tamura, T. (2012) Beach ridges and prograded beach deposits as palaeoenvironment records. Earth Science Reviews, Vol. 114, 279-297. https://10.1016/j.earscirev.2012.06.004

Tjia, H.D. (1996) Sea-level changes in the tectonically stable Malay–Thai Peninsula. Quaternary International, Vol. 31, 95–101. https://doi.org/10.1016/1040-6182(95)00025-E

Umitsu, M., Tanavud, C., Patanakanog, B. (2007) Effects of landforms on tsunami flow in the plains of Banda Aceh, Indonesia, and Nam Khem, Thailand. Marine Geology, Vol. 242, 141-153. https://doi.org/ 10.1016/j.margeo.2006.10.030

Wang, Y., Cheng, H., Edwards, L., He, Y., Kong, X., An, Z., Wu, J., Kelly, M., Dykoski, C., Li, X. (2005) The Holocene Asian Monsoon: links to solar changes and North Atlantic climate. Science, Vol. 308, 854–857. https://DOI: 10.1126/science.1106296